



We are Nitinol.™

On the Tensile and Torsional Properties of Pseudoelastic NiTi

Adler, Yu, Pelton, Zadno, Duerig, Baressi

Scripta Metallurgica et Materialia

Vol. 24

pp. 943-947

1990

ON THE TENSILE AND TORSIONAL PROPERTIES OF PSEUDOELASTIC NiTi

P.H. Adler, W. Yu, A.R. Pelton, R. Zadno, T.W. Duerig and R. Barresi
Raychem Corporation, Menlo Park, CA 94025, USA(Received February 8, 1990)
(Revised March 9, 1990)Introduction

In recent years, certain Ni-Ti and Cu-based alloys have found a wide range of applications heretofore unattainable in conventional materials by exploiting the effect known as *shape memory*. Via the shape memory effect (SME) a temperature differential or applied stress results in a martensitic transformation. The martensitic interfacial mobility in shape memory alloys (SMA) is much greater than in non-thermoelastic martensitic materials, the most common example being the TRIP (Transformation-Induced Plasticity) steels (1). Numerous studies on thermoelastic and pseudoelastic alloys cite elastic, rather than plastic, accommodation of the overall shape change as the reason shape memory alloys exhibit increased interfacial mobility (2-5).

While a number of studies have focused on the mechanical behavior of SMA under tensile loading (6-9), relatively little work has been done to characterize properties under other stress states. As a number of engineering applications involve combinations of loading states it is important to characterize material properties as a function of stress state. For example, Ni-Ti springs designed for use in thermal actuators are subjected to torsional loading when activated. Very little work has been done to describe the behavior of SMA under torsional loading conditions. Eventual development of the constitutive equations governing mechanically-induced transformations in SMA would greatly facilitate engineering design of sophisticated components. We explore here the relationships between tensile and torsional deformation of a Ni-Ti shape memory alloy.

Materials and Experimental Procedures

A Ni-49.2a/o Ti (nominal composition) alloy was prepared by electron-beam melting in a water-cooled Cu crucible. The cast material was hot swaged at 850°C then cold worked 30% to a final diameter of 17mm. Tensile samples (50.8mm gauge length and 6.35mm gauge diameter) and hollow torsion samples (15.7mm gauge length, 6.1mm outer diameter and 4.0mm inner diameter, with an enlarged grip diameter=12.7mm) were machined then stress relieved at 375°C for 30min. Differential scanning calorimetry showed the martensite start temperature $M_s = -22^\circ\text{C}$, the austenite reversion temperature $A_s = 38^\circ\text{C}$ and the transformational enthalpy $\Delta H = 208$ cal/mole for the stress-relieved material.

Uniaxial tensile tests were performed to about 0.08 true strain using an MTS servo-hydraulic testing unit with a 200kN load cell and a 1" clip-on extensometer to measure engineering strain. Measured loads and engineering strains were converted to true stress-true strain with a correction applied to the strains due to the temperature dependence of the electrical characteristics of the extensometer. Temperatures were achieved using an environmental chamber and monitored at the sample surface with a type T thermocouple. Temperature control was to $\pm 1^\circ\text{C}$. All testing was performed in air at a true strain rate of $1 \times 10^{-3} \text{s}^{-1}$.

A torsion apparatus was constructed which allowed free motion of one end of the round sample. Over the relatively small range of strains tested ($\epsilon \leq 0.08$) frictional end effects and changes in the gauge length geometry were assumed negligible. This was verified by monitoring the change in outer diameter of a sample tested at room temperature. The maximum diametral change corresponded to a change in gauge length of 0.6%. Angular displacements (θ) were measured using a rotational variable displacement transducer (RVDT) mounted at one end of the torsion apparatus. High temperature tests (100°C-200°C) were conducted using a resistance heater immersed in UCON[®] oil while room temperature and 50°C tests were performed in ethylene glycol. Low temperatures were established using liquid nitrogen (-196°C), ethyl alcohol cooled by liquid nitrogen (-100°C), and ethylene glycol cooled by liquid nitrogen (-50°C). Temperatures were controlled to $\pm 1^\circ\text{C}$ and monitored at the sample surface with a type T thermocouple. The shear strain rate used for all tests was $\dot{\gamma} = 1.73 \times 10^{-3} \text{s}^{-1}$ corresponding to an equivalent tensile strain rate of $1 \times 10^{-3} \text{s}^{-1}$.

Torsional Analysis

Raw data in the form of torque-twist (M- θ) curves were converted to equivalent stress-equivalent strain for comparison with tensile data. Shear stresses, $\tau_{\theta z}$, were determined using the equation given by Nadai (10)

for large plastic torsional strains modified for a thick-wall hollow cylinder (11):

$$3M + \theta' dM/d\theta' = 2\pi\tau_o r_o^3 [1 - (\tau_i/\tau_o)(r_i/r_o)^2] \quad (1)$$

In this equation, $\theta' = \theta/L$ where L = gauge length, τ_i and τ_o = inner and outer fiber shear stresses and, r_i and r_o = inner and outer radii. Assuming the average shear stress through the wall thickness is given by $\tau_{ave} = (\tau_o + \tau_i)/2$ and $\tau_o = c\tau_i$ with c = constant, equation (1) may be expressed in terms of τ_{ave} and c as:

$$\tau_{ave} = [(1+c)/4\pi r_o (cr_o^2 - r_i^2)] [3M + \theta' dM/d\theta'] \quad (2)$$

In the absence of a tensile flow curve initial estimates of c are typically given by r_o/r_i (11) with subsequent iterative torsion testing on differing sample geometries necessary to obtain more accurate determination of c . In the present case, however, the room temperature isothermal tensile flow behavior is known, thereby, allowing accurate estimation of c by assuming that the tensile and torsional flow curves should superpose in the transformation regime. Correlation of room-temperature torsion testing with tensile data was obtained using $c=1.24$, well within acceptable limits for the ratio of outer to inner surface shear stresses (11).

Average shear strains, γ_{ave} , were determined from $\gamma_{ave} = r_{ave} \theta' / L = r_{ave} \theta'$, with $r_{ave} = (r_o + r_i)/2$. A correction for machine compliance was applied to the shear strains using a modified version of the method described by Lee and Hart (12) for uniaxial tensile testing. This method models the total measured deformation as the sum of a purely plastic component (sample) and an elastic component (sample plus machine) thus allowing calculation of an effective "spring constant", K_m , for the elastic deformation of the torsion apparatus. Via the equation $\gamma_s^{el} = \gamma_T^{el} - \gamma_m^{el}$, where γ_s^{el} and γ_m^{el} are the elastic strains of the sample and machine and γ_T^{el} is the total measured elastic strain, the value for K_m was determined to be 63.0 GPa from a room temperature torsion test on a sample of Monel for which the shear modulus ($G=65.8$ GPa) is well known. Von Mises equivalent stresses and strains were obtained from $\bar{\sigma}_{ave} = \sqrt{3}\tau_{ave}$ and $\bar{\epsilon}_{ave} = \gamma_{ave}/\sqrt{3}$, respectively. Estimates of upper and lower bounds for $\bar{\sigma}_{ave}$ were given by $\bar{\sigma}_o$ and $\bar{\sigma}_i$, respectively, with $\bar{\sigma}_o$ and $\bar{\sigma}_i$ defined in terms of the assumptions given in equation 1 viz. $\tau_{ave} = (\tau_o + \tau_i)/2$ and $\tau_o = c\tau_i$. This defines an error in $\bar{\sigma}_{ave}$ of $\pm 10\%$.

Results and Discussion

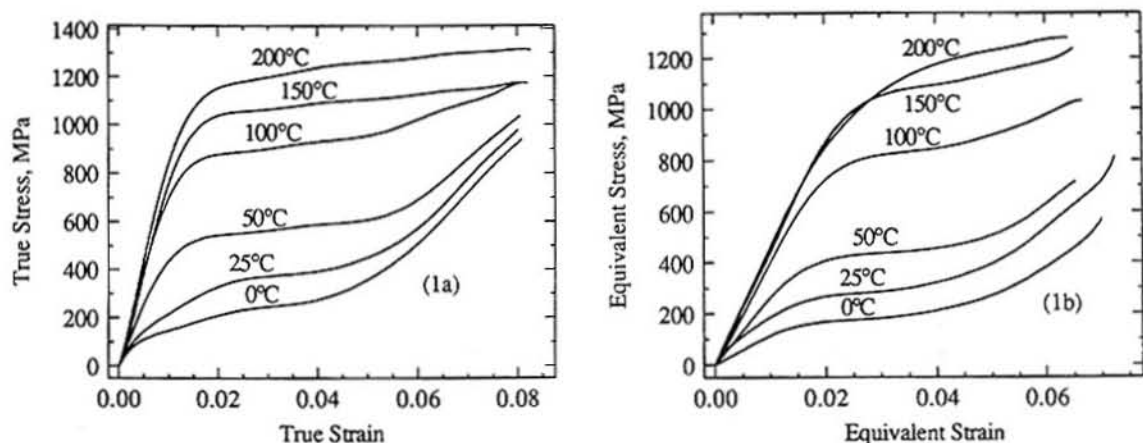
Equivalent stress-strain loading curves obtained from the tension and torsion tests over the temperature range $0^\circ\text{C} \leq T \leq 200^\circ\text{C}$ are shown in Figures 1a and 1b, while those for $-196^\circ\text{C} \leq T \leq 50^\circ\text{C}$ are presented in Figures 2a and 2b. With $M_s = -22^\circ\text{C}$, these figures show the flow characteristics of the cubic austenite (B2) and the monoclinic (B19') martensite for both stress states. The overall stress levels and trends of curve shape with temperature are in reasonable agreement with similar work performed by others (13-15).

Over the temperature range investigated three different flow regimes are identifiable: for $0^\circ\text{C} \leq T \leq 100^\circ\text{C}$ yielding occurs via stress-assisted B2 \rightarrow B19' martensitic transformation. Examination of the resulting flow curves shows two major factors controlling subsequent plastic-flow behavior: a dynamic softening effect due to the transformation acting as a deformation mechanism at low strains, followed at higher strains by a static hardening contribution of the transformation product¹. These combined effects alter the true stress-strain curves to an upward-curving shape approximating ideal exponential hardening behavior which imparts maximum stability of the macroscopic flow behavior (1). At $T \leq 50^\circ\text{C}$, the flow curves show 'rubber-like' behavior (4) reminiscent of the transformation curves in Figures 1a and 1b. In this case, however, the softening component is the result of intervariant and twin-boundary motions, while the static hardening effect is due to the formation of a set of preferred martensitic variants. At $T \geq 150^\circ\text{C}$, the critical driving force for B2 \rightarrow B19' stress-assisted transformation cannot be met despite the thermodynamic assistance of an applied stress and flow is controlled by mechanical twinning and slip in the B2 structure (16). In non-thermoelastic alloys, M_d is defined as the highest temperature at which a mechanically-induced martensitic transformation can occur. The temperature at which deformation changes from a stress-assisted to a strain-induced mechanism is M_s^o . In non-thermoelastic alloys M_d is, thus, associated with the cessation of strain-induced transformation, rather than with stress-assisted transformation. As strain-induced transformation remains a viable mode of deformation at high temperatures in Ni-Ti alloys, it is not clear whether the cessation of martensite near 100°C in the present work denotes the temperature M_d or M_s^o . More work is necessary to determine whether a strain-induced martensitic transformation occurs in these alloys.

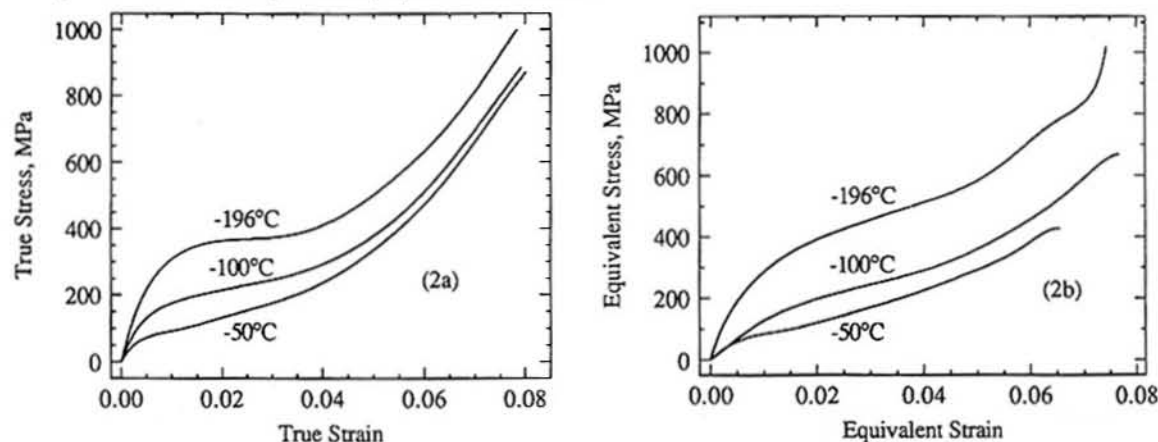
Figures 3a-c allow direct comparison of representative tensile and torsional loading and unloading flow curves in each temperature regime. Even though the strains achieved in the 50°C and 200°C torsion tests were limited to ≈ 0.065 , important quantitative information about the flow behavior at these temperatures may be obtained from these figures. Figure 4 shows the tensile and torsional yield stresses, $\bar{\sigma}_y$, as defined by the

¹The two-stage yielding phenomenon seen in the 0°C and 25°C flow curves has been described by Miyazaki and Otsuka (15) as due to either B2 \rightarrow R (commensurate) transformation or to rearrangement of R-phase variants. In either case, the temperature and strain ranges over which the R-phase exist are quite small and will not be further addressed in the present work.

intersection of the 'plateau' stress and the region of linear elasticity. Within the estimated error for $\bar{\sigma}_{ave}$ and despite an apparent difference in the elastic moduli², the $\bar{\sigma}_t$ for tension and torsion are nearly identical for a given temperature outside the transformation regime ($-50^\circ\text{C} \leq T \leq 150^\circ\text{C}$). However, within the transformation region ($0^\circ\text{C} \leq T \leq 100^\circ\text{C}$), the yield stresses in tension are nearly 24% greater than those in torsion. Stress relaxation testing by Mukherjee et al. (14) showed the increased flow stress to be related to adiabatic heating associated with the exothermic B2 \rightarrow B19' transformation occurring during tensile loading. Monitoring the surface temperature of a solid tensile sample tested in air at room temperature showed a temperature rise of $\approx 14^\circ\text{C}$ compared to a maximum temperature increase of $\approx 1^\circ\text{C}$ for the hollow torsion bar tested in agitated liquid.



FIGS. 1a and 1b. Tensile true stress-true strain loading curves (1a), and torsional equivalent stress-equivalent strain loading curves (1b) for $0^\circ\text{C} \leq T \leq 200^\circ\text{C}$.



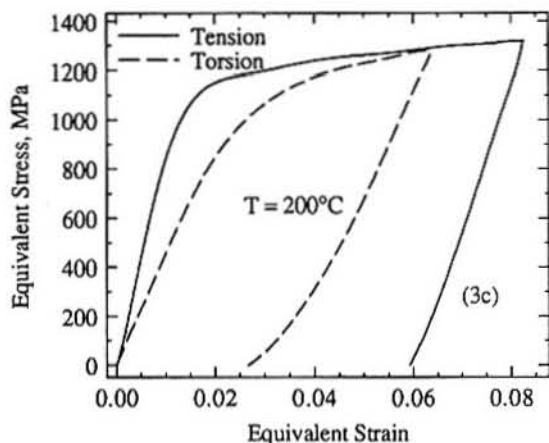
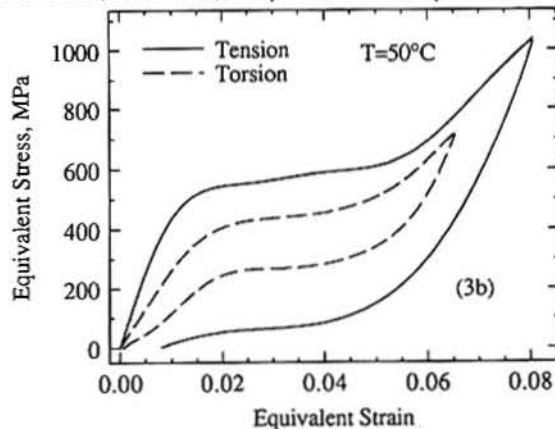
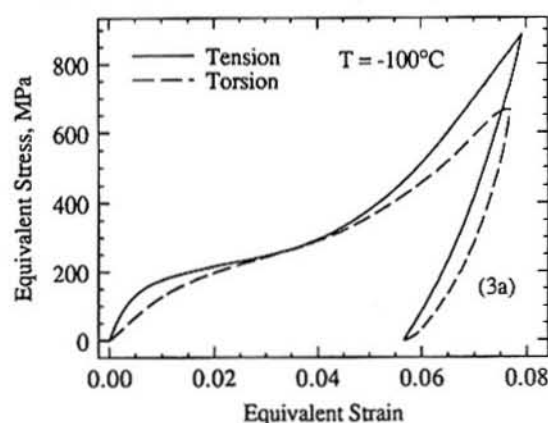
FIGS. 2a and 2b. Tensile true stress-true strain loading curves (2a), and torsional equivalent stress-equivalent strain loading curves (2b) for $-196^\circ\text{C} \leq T \leq -50^\circ\text{C}$.

A theoretical estimate of the increase in transformation stress, $\bar{\sigma}_t$, due to sample heating under adiabatic conditions is provided by the Clausius-Clapeyron relation, $d\bar{\sigma}_t/dT = -\Delta H/T\epsilon_s$. With $\Delta H = -208$ cal/mole, ϵ_s the macroscopic transformational shape strain $= 0.075$, and $T = M_s$, this relation predicts $d\bar{\sigma}_t/dT = 5.9$ MPa/ $^\circ\text{C}$ for the B2 \rightarrow B19' transformation. This prediction is 10% lower than the experimental determination of $d\bar{\sigma}_t/dT = 6.5$ MPa/ $^\circ\text{C}$ shown in Figure 4. Work by others (7) shows good agreement with the current experimental value. Using the experimental value for $d\bar{\sigma}_t/dT$, the measured increase in surface temperature of the tensile bar provides an upper limit estimate of stress increase of ≈ 90 MPa due to sample heating compared to ≈ 7 MPa for the torsion sample. As indicated in Figure 4, the average difference between the tensile and torsional yield strengths in the transformation temperature range is ≈ 82 MPa. Therefore, the experimentally determined value for

²The torsion tests described herein were not designed to accurately determine shear moduli.

$d\bar{\sigma}_y/dT$ accurately predicts the observed difference in yield stresses between tension and torsion in the temperature region of transformation.

Although the value of $d\bar{\sigma}_y/dT$ predicted by the Clausius-Clapeyron relation is close to that found in the current set of experiments, the inherent uncertainties in ΔH , T , and ϵ_0 render it prone to substantial inaccuracies. In addition, the Clausius-Clapeyron relation does not include transformational kinetic considerations and neglects stored elastic strain energy important in thermoelastic transformations. Development of the constitutive relations governing deformation-induced B2→B19' transformation would incorporate the effects of both transformation kinetics and stored elastic strain energy and, therefore, allow more accurate prediction of both $\bar{\sigma}_y$ and $d\bar{\sigma}_y/dT$ as a function of strain, strain rate, composition and temperature.



FIGS. 3a, 3b and 3c. Comparison of tension and torsion equivalent stress-strain loading and unloading curves at -100°C ($T < M_s$, fig. 3a), 50°C ($M_s < T < M_d$, fig. 3b), and 200°C ($T > M_d$, fig. 3c).

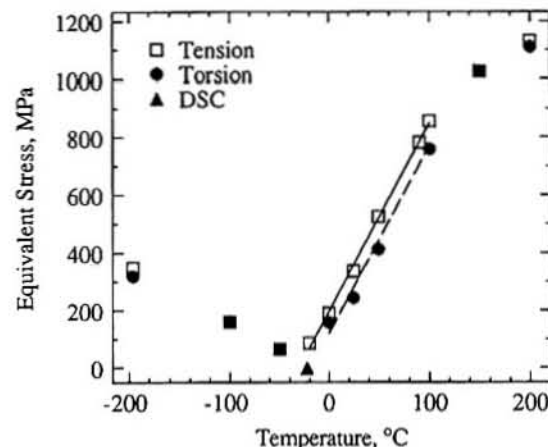


FIG. 4. Tensile (open squares) and torsional (filled circles) yield stresses for $-196^\circ\text{C} < T < 200^\circ\text{C}$. For $-22^\circ\text{C} < T \leq 100^\circ\text{C}$ i.e., in the temperature region of transformation, $(d\bar{\sigma}_y/dT)_{\text{tension}} = (d\bar{\sigma}_y/dT)_{\text{torsion}} = 6.5 \text{ MPa}/^\circ\text{C}$. See text for definition of yield stress.

Patel and Cohen (17) modeled the thermodynamic contribution of applied stress to the kinetics of stress-assisted martensitic transformation in a polycrystalline material as the sum of the resolved normal ($\sigma_n \epsilon_n$) and shear ($\tau \gamma$) work components acting through a given crystallographic variant. Since the overall shape change for the B2→B19' transformation consists primarily of shear strains, $\epsilon_n = 0$ for this transformation and, therefore, the work done in transforming a volume of cubic austenite is the same for both stress states. Theoretically, then, both the stress for transformation, $\bar{\sigma}_y$, and the temperature dependence of this stress, $d\bar{\sigma}_y/dT$, should be the same in tension and torsion for the B2→B19' transformation. Figure 4 shows the slopes of best fit lines through the experimentally determined $\bar{\sigma}_y$ to be quite similar for both tension and torsion in the temperature region of transformation, consistent with theoretical prediction.

Based on the measured temperature increase in the tensile and torsional samples, the experimental value for $d\bar{\sigma}_1/dT$ of ≈ 6.5 MPa/ $^{\circ}$ C accurately predicts the observed difference in yield strengths between tension and torsion. However, two assumptions are implicit in this prediction: that adiabatic heating occurs and that the maximum sample temperature is reached prior to macroscopic yielding. While these assumptions may, thus, allow calculation of an upper limit approximation of the increase in stress due to B2 \rightarrow B19' transformation, they do not accurately reflect experimental heat flow conditions in a transforming tensile or torsional sample. Recent stress relaxation experiments show the maximum decrease in tensile flow stress at a fixed level of strain is similar for near adiabatic or near isothermal conditions contrary to the findings of Mukherjee et al. (14). It is thought the inherent strain rate sensitivity of the B2 \rightarrow B19' martensitic transformation may play a more important role in determining the flow characteristics of this material than previously considered. Further experiments are planned to explore these phenomena in greater detail.

References

1. G.B. Olson, Deformation, Processing, and Structure, (ed. G. Krauss), p. 391, ASM (1984).
2. G.B. Olson and M. Cohen, Scripta Metall., 9, 1247 (1975).
3. G.B. Olson and M. Cohen, Scripta Metall., 11, 345 (1977).
4. M. Cohen and C.M. Wayman, Metallurgical Treatises, (ed. J.K. Tien and J.F. Elliott), p. 445, TMS-AIME (1982).
5. G.B. Olson and M. Cohen, Dislocations in Solids, vol. 7, (ed. F.R.N. Nabarro), p. 297, North-Holland, Amsterdam (1986).
6. S. Miyazaki, T. Imai, Y. Igo and K. Otsuka, Metall. Trans., 17A, 115 (1986).
7. T. Saburi, M. Yoshida and S. Nenno, Scripta Metall., 18, 363 (1984).
8. S. Miyazaki, Y. Ohmi, K. Otsuka and Y. Suzuki, Proc. Int'l. Conf. Mart. Trans (ICOMAT-82), Supplement to J. de Phys., 43, p. C4 (1982).
9. S. Miyazaki, T. Imai, K. Otsuka and Y. Suzuki, Scripta Metall., 15, 853 (1981).
10. A. Nadai, Theory of Flow and Fracture of Solids, 2nd ed., vol. 1, p. 347, McGraw-Hill (1950).
11. I. Finnie, University of California, Berkeley, private communication (1989).
12. D. Lee and E.W. Hart, Metall. Trans., 2A, 1245 (1971).
13. O. Mercier and K.N. Melton, J. Appl. Phys., 52, 1030 (1981).
14. K. Mukherjee, S. Sircar and N.B. Dahotre, Matls. Sci. Eng., 74, 75 (1985).
15. S. Miyazaki and K. Otsuka, Metall. Trans., 17A, 53 (1986).
16. E. Goo, T. Duerig, K. Melton and R. Sinclair, Acta Metall., 33, 1725 (1985).
17. J.R. Patel and M. Cohen, Acta Metall., 1, 531 (1953).

Acknowledgements

The authors are grateful for helpful discussions with Prof. G.B. Olson of Northwestern University, Evanston, IL, Prof. I. Finnie of the University of California, Berkeley, CA, Prof. A.S. Argon of the Massachusetts Institute of Technology, Cambridge, MA, and Mr. Philippe Poncet of the Metals Division, Raychem Corporation, Menlo Park, CA. We wish to thank I. Ong, C. Thomas, B. Normanly and P. Vasquez for performing the experiments.